LANGMUIR Article
Cite This: Langmuir 2017, 33, 11390-11398 pubs.acs.org/Langmuir

Stratification in Drying Polymer−Polymer and Colloid−Polymer Mixtures

Michael P. Howard,[†] Arash Nikoubashman,[‡] and Athanassios Z. Panagiotopoulos*,[†]

[†]Department of Chemical and Biological Engineering, Princeton University, Princeton, New Jersey 08544, United States of America
[‡]Institute of Physics, Johannes Gutenberg University Mainz, Staudingerweg 7, 55128 Mainz, Germany

ABSTRACT: Drying polymer−polymer and colloid−polymer mixtures were studied using Langevin dynamics computer simulations. Polymer−polymer mixtures vertically stratified into layers, with the shorter polymers enriched near the drying interface and the longer polymers pushed down toward the substrate. Colloid−polymer mixtures stratified into a polymer-on-top structure when the polymer radius of gyration was comparable to or smaller than the colloid diameter, and a colloid-on-top structure otherwise. We also developed a theoretical model for the drying mixtures based on dynamical density functional theory, which gave excellent quantitative agreement with the simulations for the polymer−polymer mixtures and qualitatively predicted the observed polymer-on-top or colloid-on-top structures for the colloid−polymer mixtures.

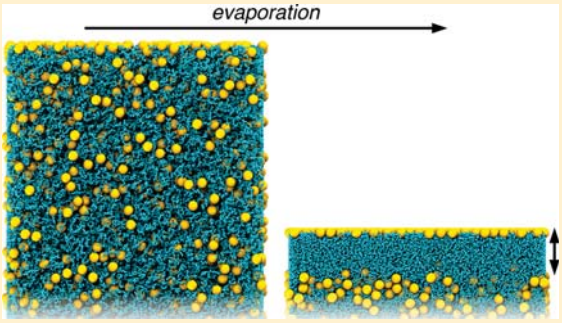

1. INTRODUCTION

In the conventional picture of latex film formation,[1,2] a liquid solvent is evaporated from a solution of initially well-dispersed colloids,[3] polymers,[4] and other additives.[2,5] Drying concentrates the solute until the colloids form a close-packed structure. The colloids deform, and an interdiffusion process creates a continuous coating. A similar drying mechanism is relevant to many technologies, including inkjet printing and the fabrication of polymer LED displays.[6−9] In all these scenarios, it is important to control the drying process in order to engineer the structure and properties of the deposited film.[10,11]

In particular, mixtures of colloids with different sizes can nontrivially stratify into vertically segregated layers during drying.[11] Such stratification may be beneficial for single-step deposition of a multilayer coating but could be detrimental if a homogeneous coating is instead required. Recent experiments and computer simulations have shown that mixtures of large and small colloids form a layer of small colloids at the drying solvent−air interface with the larger colloids pushed to the bottom.[12−15] The thickness of the stratified layer of small colloids can be controlled through the particle size asymmetry and drying rate.[13,14] Polydisperse colloidal mixtures also undergo a similar stratification, forming a gradient distribution of colloids based on their diameters.[15]

Stratification with smaller colloids on top of the larger ones is peculiar because the opposite behavior might be expected based on rates of accumulation. Larger colloids have smaller diffusion coefficients than smaller colloids and so should accumulate faster at the drying solvent−air interface in an *ideal* solution. However, additional *nonideal* interactions between the small and large colloids induce a larger migration velocity on the larger colloids, giving rise to the observed inverted stratification. Fortini et al. hypothesized that this behavior was caused by an osmotic pressure gradient.[12] Zhou et al. recently proposed an alternative diffusion model using the chemical potential gradient for a dilute colloid mixture as the driving force[16] and demonstrated that colloid cross-interactions cause inverted stratification. We concurrently proposed a model[14] based on a nonlocal density functional theory that is valid for a larger range of colloid densities and density gradients than the Zhou et al. model,[16] and we performed extensive computer simulations of the drying dynamics to show that our theory correctly predicted scaling relations for the migration velocities.[14]

Despite these recent advances for mixtures of hard colloids, relatively little is known about how polymers and other soft materials stratify during drying. Stratification has been proposed as a key step in the mechanism for phase separation[17,18] of spin-coated thin-films of immiscible polymer blends.[19] In polydisperse mixtures, stratification may modify the distribution of polymers at the drying interface, affecting the drying dynamics[20] and film structure[21,22] through the polymer skin-layer.[23−25] Processing conditions can also be exploited to control the dispersion of nanoparticles in polymer nanocomposites.[26,27] Cheng and Grest[28] showed that polymers can form a protective layer that prevents aggregation of colloids at the drying interface and increases colloid dispersion toward the substrate. However, their study was restricted to a regime in which the nanoparticles were larger than the polymers. In short,

Special Issue: Tribute to Keith Gubbins, Pioneer in the Theory of Liquids

Received: June 17, 2017
Revised: August 4, 2017
Published: August 9, 2017

DOI: 10.1021/acs.langmuir.7b02074
Langmuir 2017, 33, 11390−11398

there are many potential applications and implications of stratification for polymers in drying films, but additional understanding is first required.

In this article, we investigate stratification during drying of both polymer−polymer and colloid−polymer mixtures. We propose a predictive theoretical model for stratification in these mixtures and perform computer simulations to validate our model. We demonstrate excellent agreement between the model predictions and the simulations for the polymer−polymer mixtures, which undergo an inverted stratification with the shorter polymer chains found on top. We show that colloid−polymer mixtures exhibit either colloid-on-top or polymer-on-top stratification and that this stratification can be predicted theoretically based on the relative sizes of the polymers and colloids. Our results have implications for the engineering of multilayer coatings, polymer nanocomposites, and organic electronics.

The rest of the article is organized as follows. The physical problem is motivated and described in Section 2, and the corresponding simulation model and methods are presented. The theoretical model for the drying mixtures is developed in Section 3. The model predictions and simulation results are then compared and discussed in Section 4.

2. SIMULATION MODEL AND METHODS

Linear polymer chains in solution were modeled as M beads connected by springs. Monomers of diameter d and mass m interacted with each other through the purely repulsive Weeks−Chandler−Andersen potential,[29]

$$U_{\mathrm{nb}}(r) = \begin{cases} 4\varepsilon\left[\left(\frac{\sigma}{r}\right)^{12} - \left(\frac{\sigma}{r}\right)^{6} + \frac{1}{4}\right] & r < 2^{1/6}\sigma \\ 0 & r \geq 2^{1/6}\sigma \end{cases} \quad (1)$$

where r is the distance between the centers of two monomers, ε sets the strength of the repulsion, and $\sigma = d$. Bonds between monomers were modeled using the finitely extensible-nonlinear-elastic potential,[30]

$$U_{\mathrm{b}}(r) = \begin{cases} -\frac{\kappa r_0^2}{2}\ln\left[1 - \left(\frac{r}{r_0}\right)^2\right] & r < r_0 \\ \infty & r \geq r_0 \end{cases} \quad (2)$$

with the standard Kremer−Grest parameters $\kappa = 30\varepsilon/d^2$ and $r_0 = 1.5d$.[31] These parameters give an equilibrium bond length $b \approx 0.97d$ at temperature $T = \varepsilon/k_{\mathrm{B}}$ (k_{B} is Boltzmann's constant), which prevents any unphysical chain-crossing. In a dilute solution, this polymer model approximately corresponds to good solvent conditions, for which the polymer radius of gyration R_{g} is given by $R_{\mathrm{g}} \sim bM^{\nu}$ with $\nu \approx 0.588$ in the large M limit.[32]

As in our previous work,[14] interactions between colloids of diameter d_{c} and mass m_{c} were also modeled using eq 1 with $\sigma = d_{\mathrm{c}}$ for colloid−colloid interactions and $\sigma = (d_{\mathrm{c}} + d)/2$ for colloid−monomer interactions. The colloid mass was scaled relative to the monomer mass by volume, $m_{\mathrm{c}} = (d_{\mathrm{c}}/d)^3\, m$. The systems were bounded below by a smooth substrate that was modeled with a purely repulsive potential. Because explicitly resolving the solvent would be highly computationally intensive, the solvent was instead represented implicitly using Langevin dynamics simulations.[33−35] This simulation method includes the effects of Brownian motion and solvent drag but neglects other hydrodynamic interactions. The solvent−air interface was represented using the purely repulsive part of a harmonic potential. Gravity did not act on any of the components of the mixture. A detailed description of the model parameters (using the monomer diameter as the unit of length) can be found in ref 14.

For a single polymer chain, the Langevin equations of motion give rise to Rouse-like scaling[36] for the center-of-mass diffusion coefficient, $D = k_{\mathrm{B}}T/M\gamma$, where γ is the friction coefficient imposed on a monomer in the simulation. However, hydrodynamic interactions for polymer chains in dilute solution should instead result in Zimm-like scaling,[32,37−39]

$$D = \frac{k_{\mathrm{B}}T}{M\gamma} + \frac{k_{\mathrm{B}}T}{6\pi\eta}\left\langle\frac{1}{R_{\mathrm{h}}}\right\rangle \quad (3)$$

where η is the solution viscosity and R_{h} is the hydrodynamic radius of the polymer,

$$\left\langle\frac{1}{R_{\mathrm{h}}}\right\rangle = \frac{1}{M^2}\sum_{i\neq j}^{M}\left\langle\frac{1}{r_{ij}}\right\rangle \quad (4)$$

with r_{ij} being the distance between monomer i and monomer j in the polymer chain. The hydrodynamic radius is proportional to the radius of gyration ($R_{\mathrm{h}} \sim R_{\mathrm{g}} \sim bM^{\nu}$),[40] and so from eq 3, the diffusion coefficient scales as $D \sim k_{\mathrm{B}}T/\eta bM^{\nu}$ in the large M limit. This Zimm-like scaling has a weaker M dependence ($D \sim 1/M^{\nu}$) than Rouse-like scaling ($D \sim 1/M$).

In order to approximately obtain Zimm-like scaling for D in our Langevin dynamics simulations, we adjusted γ to depend on M:

$$\gamma = \gamma_0\left(1 + M\left\langle\frac{d}{2R_{\mathrm{h}}}\right\rangle\right)^{-1} \quad (5)$$

where we used $\gamma_0 = 3\pi\eta d$ for the low-Reynolds-number motion of a spherical monomer. The hydrodynamic radius was calculated for a single chain of length M at infinite dilution (Figure 1) in order to determine γ. The polymer dynamics obtained by this procedure serve as an approximation of the true dynamics for two reasons: (1) the internal polymer dynamics in our Langevin simulations are still Rouse-like rather than Zimm-like,[31] and (2) the true polymer dynamics should cross over to Rouse-like dynamics at sufficiently high concentrations.[32] The first approximation is well-justified because the internal relaxation times of the polymers in our model are much shorter than the drying time. The second approximation is appropriate provided that the polymer solution is sufficiently dilute. Accordingly, we conducted all simulations below the estimated overlap concentration. Both of these points are discussed in more detail below.

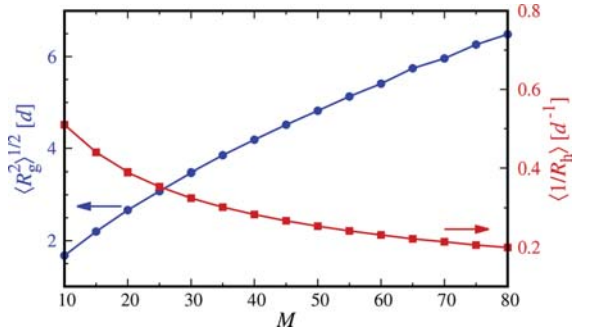

Figure 1. Radius of gyration (left axis) and inverse hydrodynamic radius (right axis) for a single polymer chain of length M at infinite dilution.

All simulations were performed using the HOOMD-blue simulation package (version 2.1.5) on general-purpose graphics processing units.[41−43] The temperature was fixed at $T = \varepsilon/k_{\mathrm{B}}$, and the simulation time step was set to 0.005τ, where $\tau = \sqrt{md^2/\varepsilon}$ is the derived unit of time. The simulation box was periodic along the x- and y-axes with edge length $L = 150\ d$. The initial interface height was $H_0 = 300\ d$.

We considered three types of mixtures: (1) a mixture of a polymer with its own monomers, (2) a mixture of two polymers, and (3) a

DOI: 10.1021/acs.langmuir.7b02074
Langmuir 2017, 33, 11390−11398

mixture of colloids and polymers. The polymer−monomer and polymer−polymer mixtures consisted of 800000 total monomers, with the monomers divided equally between the two species. The colloid−polymer mixtures were prepared from 400000 monomers and 4000 colloids with diameter $d_c = 6\ d$. We considered polymers of length M = 10, 25, 40, and 80, giving between 40000 and 5000 polymer chains of a given length and spanning a factor of 4 in R_g (Figure 1). For the colloid−polymer mixtures, the size ratio of the colloid to the polymer, $d_c/2R_g$, spans a factor of 2 with $d_c \approx 2R_g$ for M = 25. Starting configurations were generated from initially randomized states by equilibrating for 25000 τ with the friction coefficients set to $\gamma_c = \gamma$ = 0.1 m/τ in order to promote fast diffusion. Initial equilibration was confirmed by monitoring the density profiles computed with bin width 1.0 d.

Drying was simulated by moving the solvent−air interface downward with a constant speed v to a final height H = 100 d. The friction coefficient of a free monomer was set to $\gamma_0 = 2.5\ m/\tau$, which fixes the viscosity η and the effective friction coefficient γ of a polymer chain. The colloid friction coefficient γ_c was scaled relative to γ_0 by the colloid diameter, $\gamma_c = (d_c/d)\gamma_0$, according to the Stokes−Einstein relationship. For this choice of parameters, the estimated Zimm relaxation time, τ_Z, for the longest polymer chain (M = 80) was $\tau_Z \sim \eta R_g^3/k_BT \approx 71\ \tau$. The solvent-air interface typically moved with a speed $v = 2 \times 10^{-2}\ d/\tau$, and so the time required for the interface to dry a distance R_g was 324 $\tau > \tau_Z$. The estimated overlap concentration of the longest polymer chain was $c^* \sim M/R_g^3 \approx 0.3/d^3$, and so the monomer concentrations c were typically in or close to the dilute regime, $c/c^* \lesssim 1$, throughout the simulations for all chain lengths. Hence, our approximation of Zimm-like scaling for the polymer center-of-mass diffusion coefficient is reasonable.

3. THEORETICAL MODEL

The drying mixture can be modeled theoretically by a diffusion equation[14,16] within the framework of dynamical density functional theory (DDFT).[44−46] Vertical drying is essentially one-dimensional, and so the time-evolution of the colloid and polymer number density profiles, $n_i(z, t)$, is given by the conservation law,

$$\frac{\partial n_i}{\partial t} + \frac{\partial j_i}{\partial z} = 0 \tag{6}$$

where j_i is the flux for the i-th species. Both the colloids and polymers cannot cross the substrate or solvent-air interfaces. The corresponding no-flux boundary conditions are $j_i = 0$ at the substrate ($z = 0$) and $j_i = -n_i v$ at the drying solvent-air interface ($z = H_0 - vt$). With an appropriate expression for j_i, these coupled partial differential equations can be solved numerically to obtain the drying density profiles.

Under isothermal conditions, the flux is proportional to the chemical potential gradient,[46]

$$j_i = -D_i n_i \frac{\partial(\beta\mu_i)}{\partial z} \tag{7}$$

where D_i is the Stokes−Einstein diffusion coefficient and $\beta = 1/k_BT$. In DDFT, the chemical potential, $\mu_i = \delta F/\delta n_i(\mathbf{r}, t)$, is obtained by differentiation of a free-energy functional F. (Fluxes induced by gradients of other species are neglected.) In our previous work on stratification of colloid mixtures,[14] we approximated F by the White Bear version[47,48] of Rosenfeld's fundamental measure theory,[49] which gave excellent predictions for the mixture densities at equilibrium. However, obtaining the time evolution of the densities proved challenging due to nonlocal contributions to the free energy. Zhou et al.[16] modeled the same colloid mixture using a local-density approximation,[50] $F[\{n_i\}] = \int d\mathbf{r}\ f(\{n_i(\mathbf{r}, t)\})$, where f is the free-energy density. They approximated f by a virial expansion for a bulk hard-sphere mixture, which is valid in the low-density limit. This approach proved more amenable to analysis and numerical solution; however, it is expected to incur errors at moderate densities or for large density variations.

In the present work, we also adopt a local-density approximation for the free-energy functional. We will discuss the implications of this approximation later when comparing the model predictions to the simulations. The free-energy density f is obtained from the equation of state for a hard-chain mixture derived by Chapman, Jackson, and Gubbins[51,52] using Wertheim's[53−56] first-order thermodynamic perturbation theory (TPT1):

$$\beta f = \sum_i n_i \left[(\ln n_i\Lambda_i - 1) + M_i \frac{\beta f^{\mathrm{hs}}}{n_m} - (M_i - 1) \ln g(d_i^+) \right] \tag{8}$$

Each species i is considered to be a linear chain consisting of M_i hard-spheres of equal diameter d_i. (Colloids and free monomers are chains of length M_i = 1.) The first term is the free-energy density for an ideal solution of chains with thermal wavelengths Λ_i. The second term incorporates volume exclusion between colloids and monomers with f^{hs} being the excess free-energy density of a reference hard-sphere mixture with total density $n_m = \sum n_i M_i$. The last term accounts for chain formation within TPT1, where $g(d_i^+)$ is the value of the reference hard-sphere-mixture radial distribution function at contact. We model this hard-sphere mixture using Boublík's equation of state[57−59] (see Appendix A), which reduces to the accurate Carnahan−Starling equation of state[60] for the hard-sphere fluid in the case of equal diameters.

The chemical potential obtained by differentiation of the free energy has corresponding ideal and excess contributions, $\mu_i = \mu_i^{\mathrm{id}} + \mu_i^{\mathrm{ex}}$. The first term is the ideal-solution chemical potential, $\beta\mu_i^{\mathrm{id}} = \ln n_i\Lambda_i^3$. The excess chemical potential, μ_i^{ex}, contains contributions from both volume exclusion and chain connectivity. A general expression can be derived for μ_i^{ex} for the colloid−polymer mixture (see Appendix A). Qualitatively, μ_i^{ex} is proportional to chain length M_i and is larger for beads with larger diameters. For the polymer−polymer mixtures where all monomer beads have equal diameter, a particularly simple form for μ_i^{ex} is obtained:

$$\beta\mu_i^{\mathrm{ex}}/M_i = \frac{8\eta - 9\eta^2 + 3\eta^3}{(1-\eta)^3} - \left(\eta - \frac{n_p\pi d^3}{6}\right) \frac{5 - 2\eta}{(2-\eta)(1-\eta)} - \frac{M_i - 1}{M_i} \ln \frac{1 - \eta/2}{(1-\eta)^3} \tag{9}$$

where $\eta = n_m\pi d^3/6$ is the monomer packing fraction and $n_p = \sum n_i$ is the total number of polymers. The flux for a polymer chain is then

$$j_i = -D_i \left(\frac{\partial n_i}{\partial z} + n_i M_i \frac{\partial h}{\partial z} \right) \tag{10}$$

where $h(\eta, n_p) = \beta\mu_i^{\mathrm{ex}}/M_i$ is a function that is essentially independent of M_i for sufficiently long chains. The first term in eq 10 is the familiar diffusive flux and is obtained from the gradient of the ideal-solution chemical potential. The second term captures all nonideal contributions from the excess chemical potential and is necessary for stratification to occur.[14,16] The flux generates an effective migration velocity

DOI: 10.1021/acs.langmuir.7b02074
Langmuir 2017, 33, 11390−11398

$u_i = j_i/n_i$ for a polymer chain. The derivative $\partial h/\partial z$ is also independent of chain length, and so neglecting the ideal contribution, it is then clear that $u_i \sim D_i M_i$. For polymers obeying Zimm-like dynamics, $D_i \sim 1/M_i^{\nu}$ and hence $u_i \sim M_i^{1-\nu}$. Since $\nu \approx 0.588$ for good-solvent conditions, we then expect that u_i should increase as M_i increases, inducing an inverted stratification with shorter polymers on top of longer polymers.

4. RESULTS AND DISCUSSION

4.1. Polymer−polymer mixtures. We first considered the drying of polymer−monomer and polymer−polymer mixtures. Initially, the mixtures were well-dispersed with an almost uniform density distribution through the film. Near the interface, there was a small depletion of large polymers on a length scale of roughly R_g due to the entropic penalty of placing a polymer chain near an impenetrable surface. Such an equilibrium density profile is consistent with previous simulations[61] and classical density functional theory predictions.[62] The mixture drying regime can be characterized by a dimensionless Péclet number, $\mathrm{Pe}_i = H_0 v/D_i$. When $\mathrm{Pe}_i \ll 1$, diffusive motion dominates over advection, and a uniform density distribution is expected in the film; when $\mathrm{Pe}_i \gg 1$, accumulation toward the drying interface is instead expected. The monomer Péclet number was $\mathrm{Pe}_m = 15$ at the drying rate $v = 2 \times 10^{-2}\ d/\tau$. Since D_i decreases with chain length, the polymer chains had larger Pe_i than the monomers, and so both the monomers and polymers were expected to accumulate at the drying interface and form a density gradient.

Our theoretical model then predicted that inverted stratification should occur for the polymer−monomer mixtures with a layer of monomers found on top of the polymers. Figure 2 shows a snapshot for the mixture with $M = 80$ taken at the end of the simulation ($H = 100\ d$). A layer of monomers can clearly be seen on top of the polymers (Figure 2a), which have been pushed down (Figure 2b). This behavior is analogous to drying colloid mixtures,[12−15] where the larger colloids were pushed below a top layer of small colloids. We confirmed that the effect was purely nonequilibrium by stopping the drying and reestablishing nearly uniform equilibrium density profiles in the film.

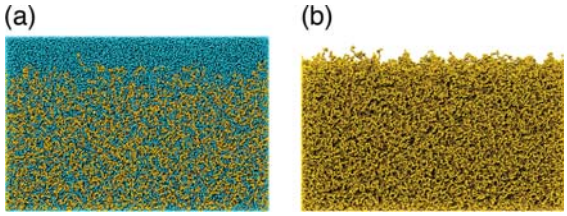

Figure 2. Snapshots of stratified 50 wt % polymer−monomer mixture for $M = 80$ at the end of drying ($H = 100\ d$) at $v = 2 \times 10^{-2}\ d/\tau$. The left image shows the entire mixture of polymers (yellow) and monomers (blue), while the right image shows only the polymers. All snapshots in this work were rendered using Visual Molecular Dynamics 1.9.3.[63]

Our theory predicts that the inverted stratification should be more pronounced for longer polymer chains because the migration velocity increases with chain length, assuming comparable density gradients in the different polymer−monomer mixtures. In order to compare the height of the stratified layer for the different mixtures, we computed the monomer density profiles, $n_{i,m}$, for both the polymers and monomers. Figure 3 shows the final density profiles obtained for the different mixtures. Consistent with Figure 2, the monomer density near the solvent−air interface was significantly higher than the polymer density, with nearly zero polymer density for the longest chains.

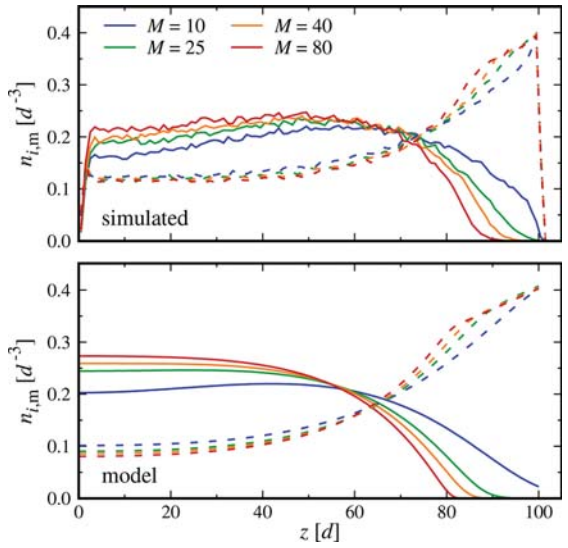

Figure 3. Final monomer density profiles for polymers of length M (solid lines) in a 50 wt % mixture with their monomers (dashed lines) dried at $v = 2 \times 10^{-2}\ d/\tau$.

The density profiles obtained by numerically solving our theoretical model for the polymer−monomer mixture (see Appendix B) are in excellent agreement with the simulation results (Figure 3). We emphasize that there are no free parameters in our theoretical model: the results were obtained by inputting only the equilibrium diffusion coefficient of a single polymer chain at infinite dilution. The density profiles predicted by the theory exhibited the same trends as the simulations, with the largest stratified layer formed for $M = 80$. The transition between the monomer-enriched top layer and the polymer-enriched bottom layer sharpened as the polymer chain length increased in both the simulations and the model, which is similar to what we observed in colloid mixtures of increasing size ratio.[14] The model also captured the sudden change in slope of the monomer density near $z \approx 80\ d$ for the $M = 80$ mixture. The theoretical model had almost perfect quantitative agreement for the maximum monomer density at the drying interface, but gave a slight overprediction of the height of the stratified layer and, as a consequence, the polymer density in the bottom of the film. One likely cause of this discrepancy is that diffusion coefficients at infinite dilution are too large compared to their actual values at finite concentration, and so the migration speeds were overpredicted. Incorporating the concentration dependence of the diffusion coefficient would likely improve this prediction. We leave such additional refinements as a subject of future work.

Polymer−polymer mixtures are also expected to stratify, using the same theoretical reasoning as for the polymer−monomer mixtures. The height of the stratified layer should be smaller when the polymer chain lengths are more similar because the difference in migration velocities is smaller. The most stratification is expected for the polymer−monomer mixture ($M = 1$), and no stratification should occur when the

DOI: 10.1021/acs.langmuir.7b02074
Langmuir 2017, 33, 11390−11398

chain lengths were equal. Figure 4 shows the final monomer density profiles for polymer−polymer mixtures with one

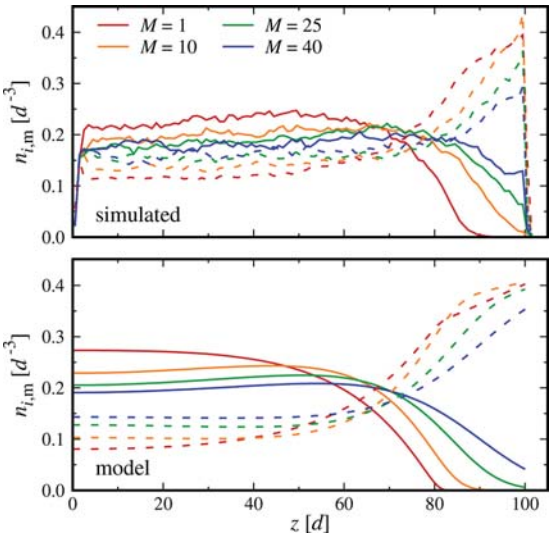

Figure 4. Final monomer density profiles for 80-bead polymers (solid lines) in a 50 wt % mixture with shorter polymers of length M (dashed lines) dried at $v = 2 \times 10^{-2}\ d/\tau$.

polymer length fixed at $M = 80$. As expected, inverted stratification occurred in all cases, but to a lesser extent for smaller chain length differences. The theoretical model again gave good quantitative predictions for the density profiles.

We expected from our theoretical model and our previous study of colloid mixtures[14] that reducing the drying speed should reduce the height of the stratified layer because the magnitude of the density gradients is reduced. To test this hypothesis, we conducted additional drying simulations for the polymer−monomer mixture with $M = 80$ at slower drying speeds $v = 2 \times 10^{-3}\ d/\tau$ and $v = 2 \times 10^{-4}\ d/\tau$. These drying speeds corresponded to $\mathrm{Pe_m} \approx 1$ and $\mathrm{Pe_m} \ll 1$ for the monomers, respectively, and $\mathrm{Pe_{80}} \gg 1$ and $\mathrm{Pe_{80}} \approx 1$ for the polymers. Minimal stratification was then expected for the slowest drying rate. Figure 5 shows the monomer density profiles at the reduced drying speeds. As expected, the height of the stratified layer decreased with v, and almost completely disappeared for the slowest drying rate. The sharpness of the stratification also decreased with decreasing drying rate, which is indeed consistent with our model and previous work.[14]

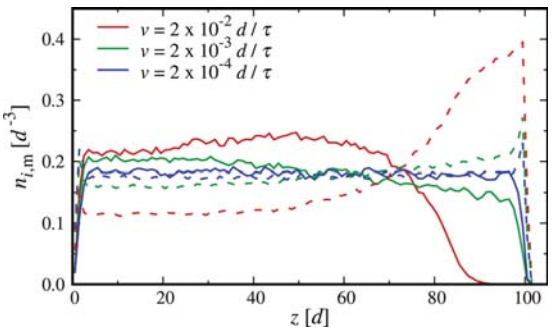

Figure 5. Final monomer density profiles for polymers of length $M = 80$ (solid lines) in a 50 wt % mixture with their monomers (dashed lines) dried at different speeds v.

Inverted stratification is predicted by our theoretical model for polymer mixtures because the driving force on the polymer increases linearly with M, while the mobility decreases like $1/M^{\nu}$ for Zimm-like diffusion. An immediate consequence of our theory is then that inverted stratification should be significantly less pronounced, or nonexistent, if the polymers instead exhibit Rouse-like diffusion, $D \sim 1/M$. We tested this prediction for the polymer−monomer mixtures by artificially setting all friction coefficients to $\gamma = \gamma_0$, which lead to Rouse-like scaling of the polymer diffusion coefficients. We found that all investigated mixtures developed similar density profiles with more polymers than monomers accumulated at the drying interface, i.e., no inverted stratification. This result highlights the important interplay between the chemical potential driving force and the mobility in determining the stratification behavior.

4.2. Colloid−polymer mixtures. We subsequently considered a mixture of colloids with diameter $d_c = 6d$ and polymers of different chain lengths. The polymer lengths were chosen to span a range of size ratios with the colloid. Making simple scaling predictions based on our theoretical model for the colloid−polymer mixture is challenging (see Appendix A); however, we can make a short qualitative analysis. At a given polymer and colloid density, the chemical potential is proportional to the chain length and is larger for larger particle diameters. The exact scaling of the chemical potential with the particle diameter is nontrivial due to the lack of a leading-order term in the diameter, but it is approximately a polynomial in d_i for a given set of volume fractions. Supposing that the scaling can be approximated as a power law of the diameter, d_i^k, the migration velocity is expected to roughly scale as $u_i \sim M_i^{1-\nu} d_i^{k-1}$ because the diffusion coefficients follow $D_i \sim 1/M_i^{\nu} d_i$ using Zimm-like scaling for the polymers or the Stokes−Einstein relation for the colloids. Provided that $k > 1$, which is reasonable for eqs 12 and 13 in Appendix A, either the polymer or the colloid will have a larger migration speed depending on the polymer chain length and the colloid diameter. When $M = 1$, the model reduces to the colloid mixture we and others previously analyzed,[12,14,16] where the smaller colloids were always found on top. Hence, we expect that short polymers ($2R_g \ll d_c$) should also stratify in a polymer-on-top configuration. In the opposite limit where the polymers are large compared to the colloids ($2R_g \gg d_c$), the colloid-on-top configuration is instead predicted. There is an intermediate value of M, when the polymer is of comparable size to the colloid, that transitions between these two regimes.

We conducted drying simulations for colloid−polymer mixtures in the high Péclet number regime. Figure 6 shows snapshots of the final dried states for polymers of length $M = 10$, $M = 25$, and $M = 80$. These polymer sizes correspond to $2R_g < d_c$, $2R_g \approx d_c$, and $2R_g > d_c$, respectively. For $M = 10$, polymer-on-top stratification occurred, and most of the colloids were pushed below the polymers, with the exception of some colloids that were trapped at the solvent−air interface before drying. This size ratio between the polymers and colloids is in a comparable regime to that studied by Cheng and Grest ($M = 100$ and $d_c = 20\ d$),[28] who also observed a similar layer of polymers on top of a drying film when the polymer−colloid interactions were weak. Polymer-on-top stratification also occurred for $M = 25$, but the separation was weaker. For $M = 80$, colloids instead aggregated at the drying interface, undergoing a colloid-on-top stratification. Hence, the polymers

DOI: 10.1021/acs.langmuir.7b02074
Langmuir 2017, 33, 11390−11398

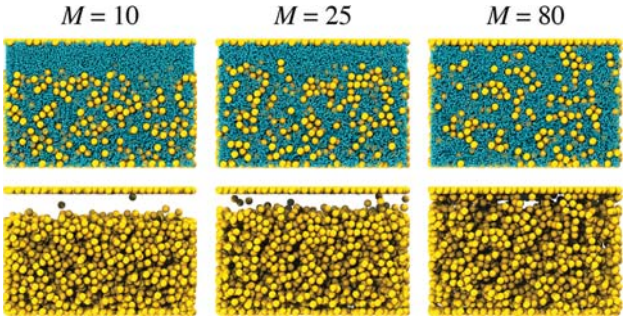

Figure 6. Snapshots of stratified colloid−polymer mixture with M = 10, 25, or 80 at the end of drying ($H = 100d$) at $v = 2 \times 10^{-2}\, d/\tau$. The top row shows the entire mixture of colloids (yellow) and polymers (blue), while the bottom row shows only the colloids.

appear to enhance the dispersion of colloids to the substrate only when $2R_g \lesssim d_c$.

The transition from polymer-on-top to colloid-on-top behavior is most readily seen in the colloid density profiles, shown in Figure 7 for the average of 40 independent drying

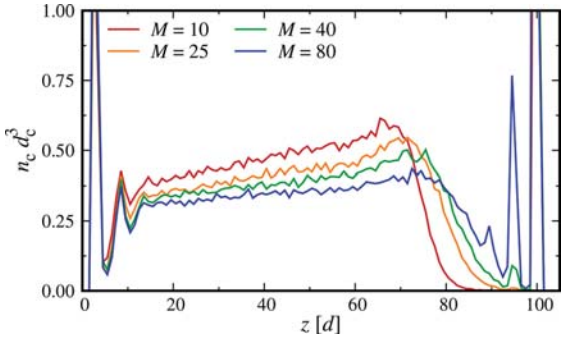

Figure 7. Final colloid density profiles for mixtures with polymers of length M dried at $v = 2 \times 10^{-2} d/\tau$.

simulations. As expected from Figure 6, polymer-on-top stratification occurred for M = 10 and M = 25. The height of the stratified layer was larger and the interface between this layer and the colloid-enriched layer was sharper for the shorter polymers. Colloid-on-top stratification occurred for both M = 40 and M = 80, and was more pronounced for the longer polymers. In both cases, a secondary peak formed at a distance of roughly d_c below the drying interface due to the accumulation of colloids at the surface. However, there was also a region below this peak that was depleted of some colloids, suggesting that some colloids were still pushed down.

We attempted to numerically solve our theoretical model for the colloid−polymer mixture and compare the final density profiles with the ones obtained from our simulations. However, our efforts were stymied by numerical instabilities at long times due to the emergence of large density gradients. We were able to resolve the early stages of drying up to time 1000 τ ($H = 280\, d$) and observed qualitatively similar trends to Figure 7. Polymer-on-top configurations were obtained for M = 10 and M = 25, and colloid-on-top configurations had already begun to form for M = 40 and M = 80. The local-density approximation for the free-energy functional was unable to resolve the multiple colloid peaks near the interface. This model could be improved by adopting a more accurate nonlocal functional,[62] which we leave as a topic for a future publication.

5. CONCLUSIONS

We developed a theoretical model for stratification in polymer−polymer and colloid−polymer mixtures, and validated it using implicit-solvent Langevin dynamics simulations. Polymer−polymer mixtures exhibited an inverted stratification analogous to colloid mixtures, with a layer of small polymers accumulated on top and larger polymers pushed down. Colloid−polymer mixtures showed polymer-on-top stratification when the polymers were smaller than the colloids ($2R_g \lesssim d_c$) and colloid-on-top stratification otherwise. Our model, based on dynamical density functional theory, predicts the nonequilibrium stratification behavior using only the equilibrium equation of state and diffusion coefficients. The model gives excellent quantitative agreement with simulations of the polymer−polymer mixtures, and qualitatively predicts both stratified structures in the colloid−polymer mixtures. Stratification of polymer−polymer mixtures and colloid−polymer mixtures has important implications for the preparation of materials such as multilayer polymer coatings or polymer nanocomposites by drying.

The analysis and simulations we performed focused on the initial stages of drying from the dilute solution regime where the polymers have Zimm-like diffusion. During the late stages of drying when the polymer concentration increases, the polymers will cross over to Rouse-like diffusion and, according to our theory and simulations, the stratified layer should cease or slow growing. If stratification is the desired effect, one could slow the polymer dynamics in order to lock in the stratified structure and prevent remixing on the time scales of additional drying, for example by increasing the viscosity of the solvent or lowering the temperature. Our theoretical model can be extended to these higher concentrations by incorporating a concentration-dependent diffusivity and a nonlocal free-energy functional. Experiments or simulations using methods capable of resolving the late stages of drying will be necessary in order to study this aspect of the process in more detail.

In the current study, we have neglected enthalpic interactions between components of the mixture. The inclusion of such interactions may alter the stratification behavior, as is true for colloid mixtures.[64] These enthalpic interactions could be incorporated into our theoretical model by appropriate modification of the free-energy functional. We have also neglected hydrodynamic interactions mediated by the solvent in our simulations or analysis. We note that Cheng and Grest obtained comparable polymer-on-top stratification for an explicit-solvent simulation of a colloid−polymer mixture,[28] and that we have also observed stratification in an explicit-solvent simulation of a polymer−polymer mixture (M = 5 and M = 15) in an unrelated study currently in progress. However, the quantitative influence of such hydrodynamic interactions on stratification is left as a subject of future work.

APPENDIX A. COLLOID−POLYMER MIXTURE MODEL

For colloid−polymer mixtures where the colloids and monomers may have different diameters, we employ Boublík's equation of state for a hard-sphere mixture.[57,58] The excess free-energy density of the mixture is[59]

DOI: 10.1021/acs.langmuir.7b02074
Langmuir 2017, 33, 11390−11398

$$\beta f^{\mathrm{hs}} = \frac{6}{\pi}\left[\left(\frac{\xi_2^3}{\xi_3^2} - \xi_0\right)\ln(1-\xi_3) + \frac{3\xi_1\xi_2}{1-\xi_3} + \frac{\xi_2^3}{\xi_3(1-\xi_3)^2}\right] \tag{11}$$

where $\xi_m = \sum_i n_i M_i \pi d_i^m/6$. (Note that ξ_3 gives the total volume fraction.) The excess chemical potential has two contributions, $\mu_i^{\mathrm{ex}} = \mu_i^{\mathrm{hs}} + \mu_i^{\mathrm{p}}$. The hard-sphere contribution μ_i^{hs} is

$$\begin{aligned}\beta\mu_i^{\mathrm{hs}}/M_i = {} & -\ln(1-\xi_3) + \frac{3\xi_2}{1-\xi_3}d_i \\ & + \left(\frac{3\xi_1}{1-\xi_3} + \frac{3\xi_2^2}{\xi_3^2}\ln(1-\xi_3) + \frac{3\xi_2^2}{(1-\xi_3)^2\xi_3}\right)d_i^2 \\ & + \left[\frac{3\xi_1\xi_2}{(1-\xi_3)^2} - \left(\frac{\xi_2^3}{\xi_3^2} - \xi_0\right)\frac{1}{1-\xi_3} - \frac{2\xi_2^3}{\xi_3^3}\ln(1-\xi_3) \right. \\ & \left. - \frac{\xi_2^3}{\xi_3^2(1-\xi_3)^2} + \frac{2\xi_2^3}{\xi_3(1-\xi_3)^3}\right]d_i^3\end{aligned} \tag{12}$$

and the chain contribution μ_i^{p} is

$$\begin{aligned}\beta\mu_i^{\mathrm{p}}/M_i = {} & -\frac{M_i-1}{M_i}\ln\left(\frac{1}{1-\xi_3} + \frac{3\xi_2 d_i}{2(1-\xi_3)^2} \right. \\ & \left. + \frac{\xi_2^2 d_i^2}{2(1-\xi_3)^3}\right) - \frac{d_i^3\pi}{6}\sum_j n_j(M_j-1) \\ & \times\left(\frac{3}{1-\xi_3} + \frac{d_j/d_i - 2}{2 + d_j\xi_2 - 2\xi_3} + \frac{d_j/d_i - 1}{1 + d_j\xi_2 - \xi_3}\right)\end{aligned} \tag{13}$$

If all diameters are equal, these expressions can be simplified to obtain eq 9 in Section 3.

APPENDIX B. NUMERICAL SOLUTION OF MODEL

We solved eq 6 numerically using the Matlab (R2016b) routine `pdepe` in a reduced set of variables. Time was reduced by the drying time for the entire film, $\tilde{t} = vt/H_0$. The spatial coordinate z was reduced by the time-dependent film height, $\tilde{z} = z/H_0(1-\tilde{t})$, which converts the shrinking domain $0 \le z \le H(t)$ to a fixed domain $0 \le \tilde{z} \le 1$. Care must be taken when transforming the time derivative into this set of coordinates. For example, for the polymer–polymer mixtures, the transformed eq 6 is

$$\frac{\partial n_i}{\partial \tilde{t}} + \frac{\tilde{z}}{1-\tilde{t}}\frac{\partial n_i}{\partial \tilde{z}} = \frac{1}{\mathrm{Pe}_i(1-\tilde{t})^2}\frac{\partial}{\partial \tilde{z}}\left(\frac{\partial n_i}{\partial \tilde{z}} + n_i M_i \frac{\partial h}{\partial \tilde{z}}\right) \tag{14}$$

The transformed boundary conditions enforce no flux at $\tilde{z} = 0$ and $\tilde{z} = 1$. We assumed that the diffusion coefficients were constant and given by their values at infinite dilution. In doing so, we neglected steric and hydrodynamic interactions at finite concentration. The hard-sphere diameters in the free-energy functional were taken to be equal to the monomer and colloid diameters because the effective hard-sphere diameters calculated for the WCA potential (eq 1) at $T = \varepsilon/k_{\mathrm{B}}$ using the mapping we employed in our previous work[14] differed by less than 2%. The density profiles were initially uniform at values consistent with the number of particles in the simulations. We solved the coupled differential equations using 100 mesh points, which we found to give acceptable numerical accuracy. The polymer density profiles were converted to monomer density profiles using $n_{i,\mathrm{m}} \approx n_i M_i$.

AUTHOR INFORMATION

Corresponding Author

*E-mail: azp@princeton.edu.

ORCID

Michael P. Howard: 0000-0002-9561-4165

Arash Nikoubashman: 0000-0003-0563-825X

Athanassios Z. Panagiotopoulos: 0000-0002-8152-6615

Notes

The authors declare no competing financial interest.

ACKNOWLEDGMENTS

Financial support for this work was provided by the Princeton Center for Complex Materials, a U.S. National Science Foundation Materials Research Science and Engineering Center (award DMR-1420541). A.N. received support from the German Research Foundation under project number NI 1487/2-1. This research is part of the Blue Waters sustained-petascale computing project, which is supported by the National Science Foundation (awards OCI-0725070 and ACI-1238993) and the state of Illinois. Blue Waters is a joint effort of the University of Illinois at Urbana–Champaign and its National Center for Supercomputing Applications. We gratefully acknowledge use of computational resources supported by the Princeton Institute for Computational Science and Engineering and the Office of Information Technology's High Performance Computing Center and Visualization Laboratory at Princeton University.

REFERENCES

(1) Keddie, J. L. Film formation of latex. *Mater. Sci. Eng., R* **1997**, *21*, 101–170.

(2) Keddie, J. L.; Routh, A. F. *Fundamentals of Latex Film Formation: Processes and Properties*; Springer: Dordrecht, 2010.

(3) Russel, W. B.; Seville, D. A.; Schowalter, W. R. *Colloidal Dispersions*; Cambridge University Press: New York, 1989.

(4) Padget, J. C. Polymers for Water-Based Coatings–A Systematic Overview. *J. Coat. Technol.* **1994**, *66*, 89–105.

(5) Hellgren, A. C.; Weissenborn, P.; Holmberg, K. Surfactants in water-borne paints. *Prog. Org. Coat.* **1999**, *35*, 79–87.

(6) Calvert, P. Inkjet Printing for Materials and Devices. *Chem. Mater.* **2001**, *13*, 3299–3305.

(7) Bale, M.; Carter, J. C.; Creighton, C. J.; Gregory, H. J.; Lyon, P. H.; Ng, P.; Webb, L.; Wehrum, A. Ink-jet printing: The route to production of full-color P-OLED displays. *J. Soc. Inf. Disp.* **2006**, *14*, 453–459.

(8) Tekin, E.; Smith, P. J.; Schubert, U. S. Inkjet printing as a deposition and patterning tool for polymers and inorganic particles. *Soft Matter* **2008**, *4*, 703–713.

(9) van Dam, D. B.; Kuerten, J. G. M. Modeling the Drying of Ink-Jet-Printed Structures and Experimental Verification. *Langmuir* **2008**, *24*, 582–589.

(10) Russel, W. B. Mechanics of Drying Colloidal Dispersions: Fluid/Solid Transitions, Skinning, Crystallization, Cracking, and Peeling. *AIChE J.* **2011**, *57*, 1378–1385.

(11) Routh, A. F. Drying of thin colloidal films. *Rep. Prog. Phys.* **2013**, *76*, 046603.

(12) Fortini, A.; Martín-Fabiani, I.; De La Haye, J. L.; Dugas, P.-Y.; Lansalot, M.; D'Agosto, F.; Bourgeat-Lami, E.; Keddie, J. L.; Sear, R. P. Dynamic Stratification in Drying Films of Colloidal Mixtures. *Phys. Rev. Lett.* **2016**, *116*, 118301.

DOI: 10.1021/acs.langmuir.7b02074
Langmuir 2017, 33, 11390–11398

(13) Martín-Fabiani, I.; Fortini, A.; Lesage de la Haye, J.; Koh, M. L.; Taylor, S. E.; Bourgeat-Lami, E.; Lansalot, M.; D'Agosto, F.; Sear, R. P.; Keddie, J. L. pH-Switchable Stratification of Colloidal Coatings: Surfaces "On Demand". *ACS Appl. Mater. Interfaces* **2016**, *8*, 34755−34761.
(14) Howard, M. P.; Nikoubashman, A.; Panagiotopoulos, A. Z. Stratification Dynamics in Drying Colloidal Mixtures. *Langmuir* **2017**, *33*, 3685−3693.
(15) Fortini, A.; Sear, R. P. Stratification and Size Segregation of Ternary and Polydisperse Colloidal Suspensions during Drying. *Langmuir* **2017**, *33*, 4796−4805.
(16) Zhou, J.; Jiang, Y.; Doi, M. Cross Interaction Drives Stratification in Drying Film of Binary Colloidal Mixtures. *Phys. Rev. Lett.* **2017**, *118*, 108002.
(17) Heriot, S. Y.; Jones, R. A. L. An interfacial instability in a transient wetting layer leads to lateral phase separation in thin spin-cast polymer-blend films. *Nat. Mater.* **2005**, *4*, 782−786.
(18) Wodo, O.; Ganapathysubramanian, B. How do evaporating thin films evolve? Unravelling phase-separation mechanisms during solvent-based fabrication of polymer blends. *Appl. Phys. Lett.* **2014**, *105*, 153104.
(19) Ebbens, S.; Hodgkinson, R.; Parnell, A. J.; Dunbar, A.; Martin, S. J.; Topham, P. D.; Clarke, N.; Howse, J. R. *In Situ* Imaging and Height Reconstruction of Phase Separation Processes in Polymer Blends during Spin Coating. *ACS Nano* **2011**, *5*, 5124−5131.
(20) Tsige, M.; Grest, G. S. Molecular Dynamics Study of the Evaporation Process in Polymer Films. *Macromolecules* **2004**, *37*, 4333−4335.
(21) Pauchard, L.; Allain, C. Buckling instability induced by polymer solution drying. *Europhys. Lett.* **2003**, *62*, 897−903.
(22) Pauchard, L.; Couder, Y. Invagination during the collapse of an inhomogeneous spheroidal shell. *Europhys. Lett.* **2004**, *66*, 667−673.
(23) de Gennes, P. G. Solvent evaporation of spin cast films: "crust" effects. *Eur. Phys. J. E: Soft Matter Biol. Phys.* **2002**, *7*, 31−34.
(24) Okuzono, T.; Ozawa, K.; Doi, M. Simple Model of Skin Formation Caused by Solvent Evaporation in Polymer Solutions. *Phys. Rev. Lett.* **2006**, *97*, 136103.
(25) Arai, S.; Doi, M. Anomalous drying dynamics of a polymer solution on a substrate. *Eur. Phys. J. E: Soft Matter Biol. Phys.* **2013**, *36*, 63.
(26) Mackay, M. E.; Tuteja, A.; Duxbury, P. M.; Hawker, C. J.; Van Horn, B.; Guan, Z.; Chen, G.; Krishnan, R. S. General Strategies for Nanoparticle Dispersion. *Science* **2006**, *311*, 1740−1743.
(27) Sen, S.; Xie, Y.; Bansal, A.; Yang, H.; Cho, K.; Schadler, L. S.; Kumar, S. K. Equivalence between polymer nanocomposites and thin polymer films: Effect of processing conditions and molecular origins of observed behavior. *Eur. Phys. J.: Spec. Top.* **2007**, *141*, 161−165.
(28) Cheng, S.; Grest, G. S. Dispersing Nanoparticles in a Polymer Film via Solvent Evaporation. *ACS Macro Lett.* **2016**, *5*, 694−698.
(29) Weeks, J. D.; Chandler, D.; Andersen, H. C. Role of Repulsive Forces in Determining Equilibrium Structure of Simple Liquids. *J. Chem. Phys.* **1971**, *54*, 5237−5247.
(30) Bishop, M.; Kalos, M. H.; Frisch, H. L. Molecular dynamics of polymeric systems. *J. Chem. Phys.* **1979**, *70*, 1299−1304.
(31) Grest, G. S.; Kremer, K. Molecular dynamics simulation for polymers in the presence of a heat bath. *Phys. Rev. A: At., Mol., Opt. Phys.* **1986**, *33*, 3628−3631.
(32) Rubinstein, M.; Colby, R. H. *Polymer Physics*; Oxford University Press: New York, 2012.
(33) Schneider, T.; Stoll, E. Molecular-dynamics study of a three-dimensional one-component model for distortive phase transitions. *Phys. Rev. B: Condens. Matter Mater. Phys.* **1978**, *17*, 1302−1322.
(34) Allen, M. P.; Tildesley, D. J. *Computer Simulation of Liquids*; Oxford University Press: New York, 1991.
(35) Phillips, C. L.; Anderson, J. A.; Glotzer, S. C. Pseudo-random number generation for Brownian Dynamics and Dissipative Particle Dynamics simulations on GPU devices. *J. Comput. Phys.* **2011**, *230*, 7191−7201.
(36) Rouse, P. E. A Theory of the Linear Viscoelastic Properties of Dilute Solutions of Coiling Polymers. *J. Chem. Phys.* **1953**, *21*, 1272−1280.
(37) Zimm, B. H. Dynamics of Polymer Molecules in Dilute Solution: Viscoelasticity, Flow Birefringence and Dielectric Loss. *J. Chem. Phys.* **1956**, *24*, 269−278.
(38) Dünweg, B.; Grest, G. S.; Kremer, K. In *Numerical Methods for Polymeric Systems*; Whittington, S. G., Ed.; The IMA Vol.s in Mathematics and its Applications; Springer: New York, 1998; Vol. *102*; pp 159−195.
(39) Doi, M.; Edwards, S. F. *The Theory of Polymer Dynamics*; Oxford University Press: New York, 1986.
(40) Teraoka, I. *Polymer Solutions: An Introduction to Physical Properties*; Wiley: New York, 2002.
(41) Anderson, J. A.; Lorenz, C. D.; Travesset, A. General purpose molecular dynamics simulations fully implemented on graphics processing units. *J. Comput. Phys.* **2008**, *227*, 5342−5359.
(42) Glaser, J.; Nguyen, T. D.; Anderson, J. A.; Lui, P.; Spiga, F.; Millan, J. A.; Morse, D. C.; Glotzer, S. C. Strong scaling of general-purpose molecular dynamics simulations on GPUs. *Comput. Phys. Commun.* **2015**, *192*, 97−107.
(43) Howard, M. P.; Anderson, J. A.; Nikoubashman, A.; Glotzer, S. C.; Panagiotopoulos, A. Z. Efficient neighbor list calculation for molecular simulation of colloidal systems using graphics processing units. *Comput. Phys. Commun.* **2016**, *203*, 45−52.
(44) Marconi, U. M. B.; Tarazona, P. Dynamic density functional theory of fluids. *J. Chem. Phys.* **1999**, *110*, 8032−8044.
(45) Archer, A. J.; Evans, R. Dynamical density functional theory and its application to spinodal decomposition. *J. Chem. Phys.* **2004**, *121*, 4246.
(46) Archer, A. J. Dynamical density functional theory: binary phase-separating colloidal fluid in a cavity. *J. Phys.: Condens. Matter* **2005**, *17*, 1405−1427.
(47) Roth, R.; Evans, R.; Lang, A.; Kahl, G. Fundamental measure theory for hard-sphere mixtures revisited: the White Bear version. *J. Phys.: Condens. Matter* **2002**, *14*, 12063−12078.
(48) Yu, Y.-X.; Wu, J. Structures of hard-sphere fluids from a modified fundamental-measure theory. *J. Chem. Phys.* **2002**, *117*, 10156.
(49) Rosenfeld, Y. Free-Energy Model for the Inhomogeneous Hard-Sphere Fluid Mixture and Density-Functional Theory of Freezing. *Phys. Rev. Lett.* **1989**, *63*, 980−983.
(50) Tarazona, P.; Cuesta, J. A.; Martínez-Ratón, Y. In *Theory and Simulation of Hard-Sphere Fluids and Related Systems*; Mulero, A., Ed.; Lecture Notes in Physics; Springer: Berlin, 2008; Vol. *753*; Chapter 7, pp 247−341.
(51) Jackson, G.; Chapman, W. G.; Gubbins, K. E. Phase equilibria of associating fluids: Spherical molecules with multiple bonding sites. *Mol. Phys.* **1988**, *65*, 1−31.
(52) Chapman, W. G.; Jackson, G.; Gubbins, K. E. Phase equilibria of associating fluids: Chain molecules with multiple bonding sites. *Mol. Phys.* **1988**, *65*, 1057−1079.
(53) Wertheim, M. S. Fluids with Highly Directional Attractive Forces. I. Statistical Thermodynamics. *J. Stat. Phys.* **1984**, *35*, 19−34.
(54) Wertheim, M. S. Fluids with Highly Directional Attractive Forces. II. Thermodynamic Perturbation Theory and Integral Equations. *J. Stat. Phys.* **1984**, *35*, 35−47.
(55) Wertheim, M. S. Fluids with Highly Directional Attractive Forces. III. Multiple Attraction Sites. *J. Stat. Phys.* **1986**, *42*, 459−476.
(56) Wertheim, M. S. Fluids with Highly Directional Attractive Forces. IV. Equilibrium Polymerization. *J. Stat. Phys.* **1986**, *42*, 477−492.
(57) Boublík, T. Hard-Sphere Equation of State. *J. Chem. Phys.* **1970**, *53*, 471−472.
(58) Mansoori, G. A.; Carnahan, N. F.; Starling, K. E.; Leland, T. W., Jr. Equilibrium Thermodynamic Properties of the Mixture of Hard Spheres. *J. Chem. Phys.* **1971**, *54*, 1523−1525.
(59) MacDowell, L. G.; Virnau, P.; Müller, M.; Binder, K. Critical lines and phase coexistence of polymer solutions: A quantitative

DOI: 10.1021/acs.langmuir.7b02074
Langmuir 2017, 33, 11390−11398

comparison between Wertheim's thermodynamic perturbation theory and computer simulations. *J. Chem. Phys.* **2002**, *117*, 6360−6371.
(60) Carnahan, N. F.; Starling, K. E. Equation of State for Nonattracting Rigid Spheres. *J. Chem. Phys.* **1969**, *51*, 635−636.
(61) Yethiraj, A.; Hall, C. K. Monte Carlo simulation of hard chain-hard sphere mixtures in slitlike pores. *J. Chem. Phys.* **1989**, *91*, 4827−4837.
(62) Yu, Y.-X.; Wu, J. Density functional theory for inhomogeneous mixtures of polymeric fluids. *J. Chem. Phys.* **2002**, *117*, 2368−2376.
(63) Humphrey, W.; Dalke, A.; Schulten, K. VMD: Visual Molecular Dynamics. *J. Mol. Graphics* **1996**, *14*, 33−38.
(64) Atmuri, A. K.; Bhatia, S. R.; Routh, A. F. Autostratification in Drying Colloidal Dispersions: Effect of Particle Interactions. *Langmuir* **2012**, *28*, 2652−2658.

DOI: 10.1021/acs.langmuir.7b02074
Langmuir 2017, 33, 11390−11398